

TASSO RESULTS ON e^+e^- ANNIHILATION BETWEEN 13 AND 31.6 GEV AND EVIDENCE FOR THREE JET EVENTS.

TASSO Collaboration

Aachen, Bonn, DESY, Hamburg, Imperial College, Rutherford, Oxford, Weizmann, Wisconsin¹⁾
Presented by G. Wolf, Deutsches Elektronen-Synchrotron DESY, Hamburg

Summary

Hadron production by e^+e^- annihilation was analyzed for c.m. energies from 13 up to 31.6 GeV at PETRA. Results are reported on R and on gross features of the final states such as multiplicity and inclusive momentum spectra. No evidence was found for a contribution of the top quark. Jet formation was studied in detail. The transverse momentum of hadrons relative to the jet axis was found to increase strongly with c.m. energy. The broadening of the jets is not uniform in the azimuthal angle around the jet axis but tends to yield planar events with large and growing transverse momenta in the plane and small transverse momenta normal to the plane. The simple qq jet picture is ruled out. The observation of planar events shows that there are three basic constituents which turn into hadron jets. Indeed, several events with three well separated jets of hadrons were observed at the highest energies. The data can be naturally understood in terms of hard gluon bremsstrahlung, with the quarks and gluons fragmenting into hadrons with limited transverse momenta.

Introduction

We report results on hadron production in e^+e^- annihilation at c.m. energies between 13 and 31.6 GeV. They were obtained with the TASSO detector at the DESY storage ring PETRA. The most important result of the analysis presented below is the evidence found for three jet events which find a natural explanation in terms of hard gluon bremsstrahlung. First evidence for this new type of process has already been reported from this experiment elsewhere². Some of the results obtained at 13 and 17 GeV have been published in Ref. 3.

1. The TASSO Detector

The experimental setup has been described in detail previously³. Fig. 1 shows a cross section of the TASSO detector. It consists of a large magnetic solenoid filled with and surrounded by tracking chambers and shower counters, plus two counter hodoscopes (= hadron arms) designed for particle identification up to the highest momenta. A luminosity monitor, which measures small angle Bhabha scattering, consists of eight counter telescopes mounted symmetrically with respect to the beam line and interaction point.

The solenoid is 440 cm in length, 135 cm in radius and produces a field of 0.5 Tesla parallel to the beam axis. Emerging from the interaction point a particle traverses the beam pipe and one of 4 scintillation counters, which form a cylinder around the beam pipe, before entering a low mass cylindrical proportional chamber, a drift chamber and a set of 48 time-of-flight counters. The proportional chamber has four gaps each containing anode wires parallel to the beam axis and two layers of cathode strips with a pitch angle of 36.5° . The efficiency of the anode wires was 97 %. The drift chamber contains 15 layers, 9 with sense wires parallel to the axis and 6 with sense wires oriented at approximately $\pm 40^\circ$ to the axis. The efficiency of each layer was found to be 96 %. The position resolution is approximately $280 \mu\text{m}$ which leads to a momentum resolution of $\Delta p/p \approx 2\% \cdot P$. (P in GeV/c). The data were obtained with the following trigger: a coincidence between beam pick up signal, any beam pipe counter and any TOF counter together with information from 6 of the 9 zero

degree layers of the drift chamber gated into a hard-wired logic unit. This unit searched for tracks and determined their transverse momenta. Simultaneously the hits in the proportional chamber were gated into a separate processor which searched for track segments. A track was finally defined as the coincidence between a track from the drift chamber processor, a track segment from the proportional chamber processor and the corresponding TOF counter. The trigger demanded either two tracks coplanar with respect to the beam axis or at least four tracks. The transverse momentum of these tracks was required to exceed 320 MeV/c. The resulting trigger rate was in the range 1-2 Hz. Fig. 2 shows a typical multihadron event as registered in the central detector.

The luminosity was determined from measurements of the Bhabha cross-section at small angles. Large angle Bhabha scattering observed in the central detector was found to be consistent within the errors with the small angle result.

2. Selection of Multihadron Events

The selection of multihadron events was done in two steps:
At least 3 tracks were required in the projected r - φ plane (perpendicular to the beam axis) with at least 2 fully reconstructed in three dimensions. The three tracks have $d < 2.5 \text{ cm}$ and $|z| < 10 \text{ cm}$, where d is the distance of closest approach in the r - φ plane and z is the z coordinate at the point of closest approach to the z axis=beam axis. Furthermore at least one charged track must be in each of the two hemispheres oriented along the beam direction and the sum of the absolute values of the momenta should exceed 1 GeV.

In the second step these events were examined visually. To be considered in the following analysis a charged track must have had a transverse momentum of 100 MeV/c and reached at least the sixth zero-degree layer of the drift chamber. This imposes an angular cut of $|\cos\theta| \leq 0.87$. τ candidates were removed.

Fig. 3 shows the distribution of ΣP_i where P_i is the momentum of a charged track and the sum is extended over all tracks accepted for a given event. The event vertex was required to be close to the interaction point, $|z| < 10 \text{ cm}$. Data taken at total c.m. energies W of 27.4, 27.7 (average value 27.6 GeV), 30.0 and 31.6 GeV were combined in this plot.

The excess of events at low ΣP_i is due to beam gas scattering and $\gamma\gamma$ interactions. The beam gas contribution was estimated from an analysis of events outside of the interaction region, $10 < |z| < 30 \text{ cm}$. The result is shown by the dashed histogram. The events from the one photon annihilation channel populate the high ΣP_i region. For the further analysis ΣP_i was required to exceed a certain minimum value W_{min} which for the data shown in Fig. 3 was chosen to be 9 GeV. This provides a clean sample of one photon events.

The curve shown in Fig. 3 was calculated using a 2 jet Monte Carlo program⁴ that took into account the acceptance of the detector and the selection criteria. The Monte Carlo curve describes the event distribution above W_{min} rather well.

Table I lists for the six energies at which data were taken the luminosity and the number of multihadron events observed above W_{min} .

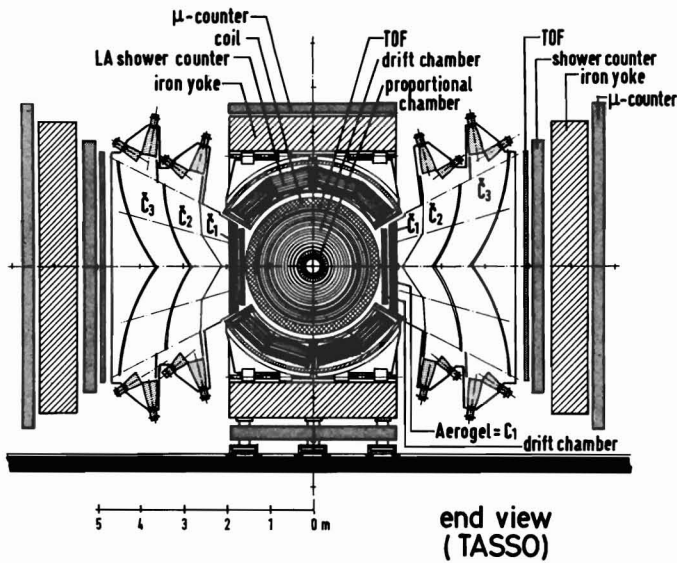


Fig.1 The TASSO detector viewed along the beam.

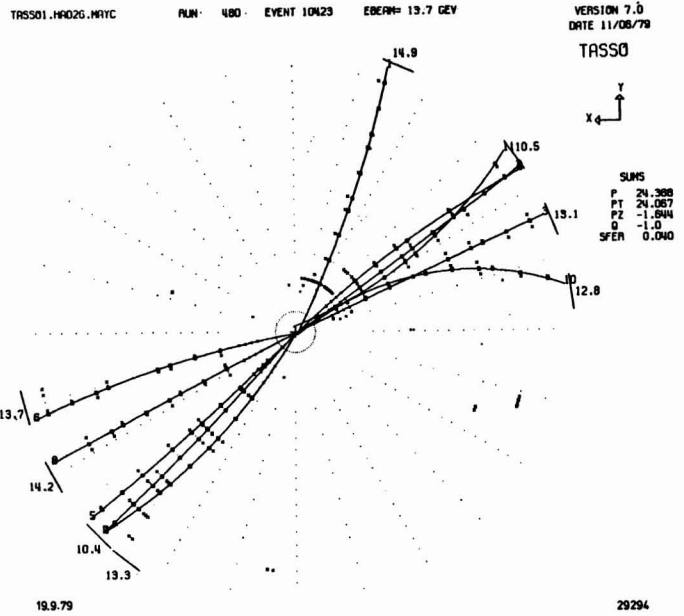


Fig.2 A typical multihadron event at 27.4 GeV recorded in the central detector. The inner 4 layers belong to the proportional chamber, the following 9 are zero degree layers of the drift chamber. The solid bars at the periphery mark time-of-flight counters.

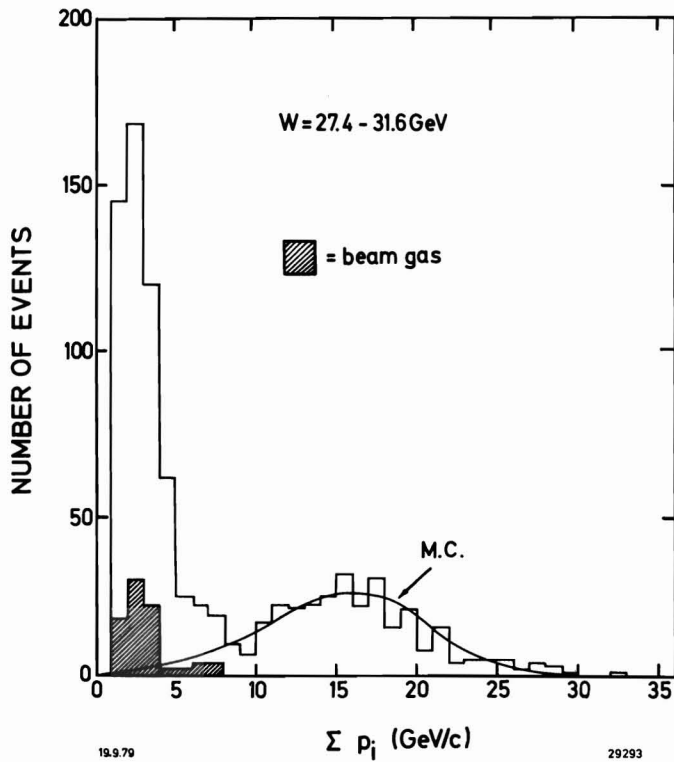


Fig.3 Distribution of the total visible momentum of the hadronic candidates. The solid curve shows the Monte Carlo prediction for hadron production through one-photon annihilation in the $q\bar{q}$ model.

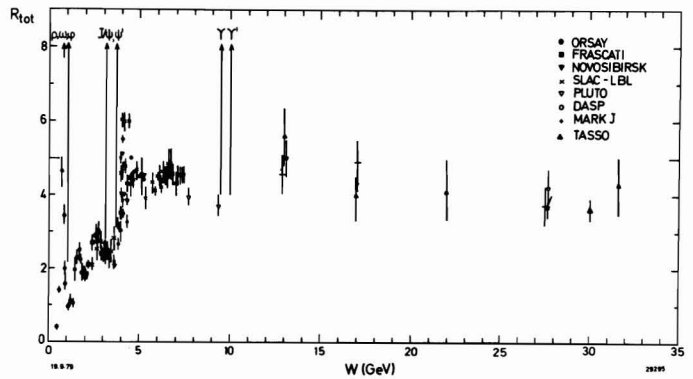


Fig.4 The ratio R of the hadronic to μ pair production cross sections as a function of the c.m. energy W .

Table I: Integrated luminosity and number of multi-hadron events with $\Sigma P_i > W_{\min}$

W (GeV)	s=W ² (GeV ²)	$\int \mathcal{L} dt$ (nb ⁻¹)	W _{min} (GeV)	number of events with $\Sigma P_i > W_{\min}$
13.	169	30.3	3	72
17	289	39.2	4	40
22	484	45.6	6	26
27.6	760	329.6	9	118
30.0	900	447.3	9	132
31.6	1000	126.1	9	40

3. Determination of R

The total cross section, σ_{tot} , for $e^+e^- \rightarrow \text{hadrons}$

was determined from the number of multihadron events observed above W_{\min} . Corrections were applied for contributions from beam gas scattering, $\gamma\gamma$ scattering and $\tau\bar{\tau}$ production. The detection efficiency as determined from the Monte Carlo program varied between 75 % and 78 %. The corrections for radiative effects amounted to -8 %.

The resulting values for $R = \sigma_{\text{tot}}/\sigma_{\mu\mu}$ ($\sigma_{\mu\mu} = \frac{4\pi}{3} \frac{\alpha^2}{s}$, cross section for μ pair production) are listed in Table 2. The errors given are the statistical ones. The relative systematic error was estimated to ± 10 %, the absolute systematic error to ± 15 %. The measurements at 13 and 17 GeV have been reported previously³.

Table 2: Measurement of R

W	R
13	5.6 \pm 0.7
17	4.0 \pm 0.7
22	4.1 \pm 0.8
27.6	3.9 \pm 0.3
30.0	3.7 \pm 0.3
31.6	4.2 \pm 0.7

Fig.4 shows a compilation of R measurements as a function of W. The data above 17 GeV are consistent with a constant R with a value close to 4. The quark model including u,d,s,c and b predicts

$$R = 3\sum e_q^2 = 3.7 \quad (1)$$

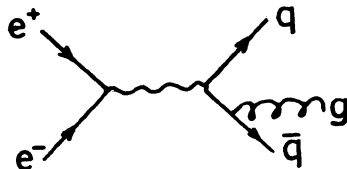
in good agreement with the data. In QCD this result is modified by gluon emission (see diagram): In first order one finds

$$R = 3\sum e_q^2 \left(1 + \frac{\alpha_s(s)}{\pi}\right) \quad (2)$$

where $\alpha_s(s)$ is the strong coupling constant,

$$\alpha_s(s) = \frac{12\pi}{(33-2N_f) \ln s/\Lambda^2} \quad (3)$$

with N_f = number of flavors and Λ a constant of order 500 MeV. The QCD correction increases the predicted R value by ~ 10 % to 4.1 which agrees also with the data.



The contribution of the hypothetical top quark t (charge 2/3) will increase R by at least 4/3 to $R > 5$ if W is above the threshold for top meson production.

The data give no evidence for the top quark.

4. Gross Features of the Final States

a) Multiplicity

The average multiplicity of charged particles $\langle n_{\text{ch}} \rangle$ was determined from the observed number of accepted charged tracks. Corrections were applied for detection efficiency and for electron tracks stemming from $\pi^0 \rightarrow \gamma\gamma$ decay with photons converting in the material in front of the drift chamber. Pions from K^0 decay are included in $\langle n_{\text{ch}} \rangle$. The measured multiplicities are shown in Fig.5. The errors shown for the TASSO points are mainly systematical in origin. Fig.5 includes also measurements of $\langle n_{\text{ch}} \rangle$ at lower energies⁵⁻⁸. The data show that the multiplicity above ~ 10 GeV is rising (logarithmically) faster than at lower energies.

The dashed curve in Fig.5 gives the energy dependence of $\langle n_{\text{ch}} \rangle$ for pp collisions⁹. The pp multiplicity is lower $\langle n_{\text{ch}} \rangle$ by 0.5 to 1 units but has almost the same behaviour with energy. In QCD the multiplicity is expected* to behave as $\langle n_{\text{ch}} \rangle = n_0 + a \exp(b/\ln s/\Lambda^2)$. The fit to the data yields

$$\langle n_{\text{ch}} \rangle = (2.8 \pm 0.5) + (0.0044 \pm 0.07) \exp((2.6 \pm 0.5)\sqrt{\ln s/\Lambda^2})$$

where $\Lambda = 0.5$ GeV was assumed. The more rapid rise of $\langle n_{\text{ch}} \rangle$ above 10 GeV may then be taken as evidence for hard gluon contributions. However, the qq model alone using for u,d,s the fragmentation functions of Field and Feynman⁴ above 5 GeV predicts an energy dependence similar to what is seen in the data.

b) Inclusive particle spectra

The differential cross section for producing a particle h with momentum and energy p,E and angle θ relative to the beam axis can be expressed in terms of two structure functions \bar{W}_1 and \bar{W}_2 which are closely related to W_1 and W_2 measured in inelastic lepton hadron scattering¹⁰:

$$\frac{d^2\sigma}{dx d\Omega} = \frac{\alpha^2}{s} \beta \times \left\{ m\bar{W}_1 + \frac{1}{4} \beta^2 \times \nu \bar{W}_2 \sin^2\theta \right\} \quad (4)$$

where m is the mass of h, $\beta = P/E$, $x = E/E_{\text{beam}} = 2E/\sqrt{s}$ and ν is the energy of the virtual photon as seen in the h rest system, $\nu = (E/m)\sqrt{s}$. After integrating over the angles one has

$$\frac{d\sigma}{dx} = \frac{4\pi\alpha^2}{s} \beta \times \left\{ m\bar{W}_1 + \frac{1}{6} \beta^2 \times \nu \bar{W}_2 \right\} \quad (5)$$

Since the first term is dominating

$$\frac{d\sigma}{dx} \approx \frac{4\pi\alpha^2}{s} \beta \times m\bar{W}_1 \quad (6)$$

The structure functions \bar{W}_1 and $\nu\bar{W}_2$ in general are functions of two variables e.g. s and the scaling variable x which corresponds to the scaling variable $x = 1/w$ used in inelastic lepton nucleon scattering. If scale invariance holds \bar{W}_1 and $\nu\bar{W}_2$ are functions of x alone and the so called scaling cross section $s/\beta d\sigma/dx$ is almost the same for all values of s.

Scaling behaviour is e.g. expected from the hypothesis of quark fragmentation. At energies large enough that particle masses can be neglected, the number of hadrons h produced by a quark q with fractional energy x, $D_q^h(x)$, is independent of s. This leads to

$$\frac{d\sigma}{dx}(e^+e^- \rightarrow q\bar{q} \rightarrow h) = \sigma_{q\bar{q}} \cdot 2D_q^h(x) = \frac{8\pi\alpha^2}{s} e_q^2 D_q^h(x) \quad (7)$$

In the present experiment the particle masses were

* J.Ellis private communication, motivated by the work for heavy quark production; W.Furmanski, R.Petronzio, S.Pokorski, CERN-TH Report 2625.

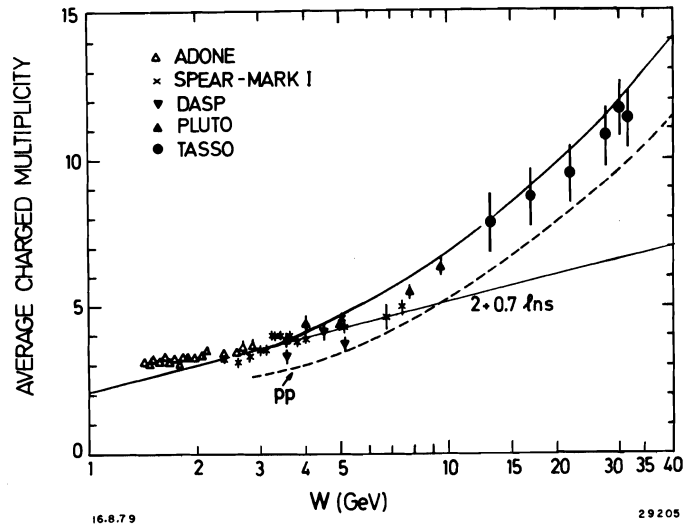


Fig.5 Average charge multiplicity from this experiment and from measurements at lower energies (Refs. 5-8). The dashed line shows the result for pp collisions (Ref. 9). The solid curve shows the result of the fit $n_{ch} = n_0 + a \exp(b\sqrt{s}/\Lambda^2)$.

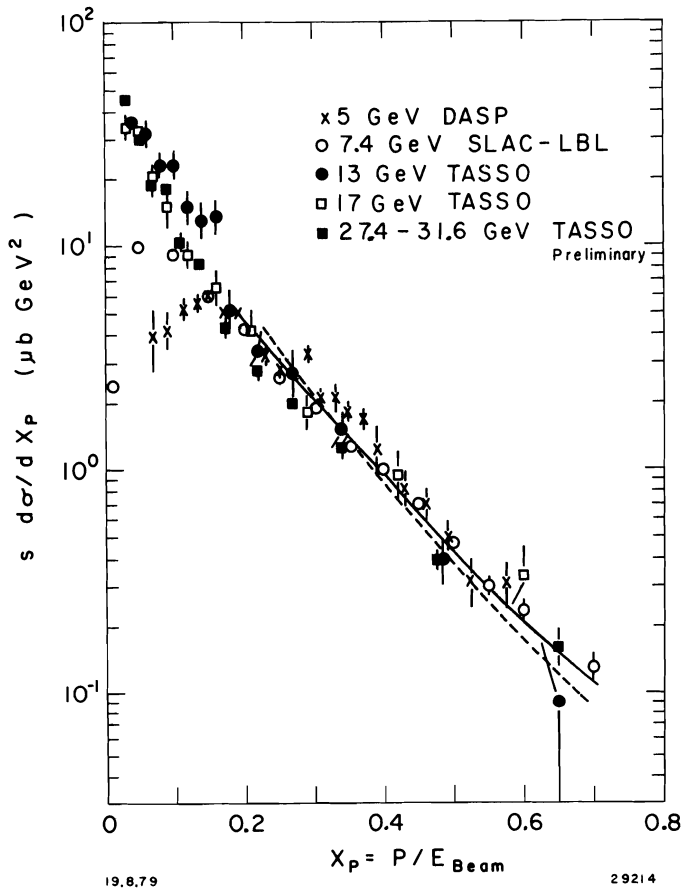


Fig.6 The scaling cross section $s d\sigma/dx$ ($x = P/E_{beam}$) for inclusive charged particle production measured in this experiment at 13, 17 and 27.4 - 31.6 GeV and at 5 GeV (DASP, Ref.8) and 7.4 GeV (SLAC-LBL, Ref. 11). The curves show the QCD scale breaking effects predicted for going from 5 GeV (solid curve) to 30 GeV (dashed curve).

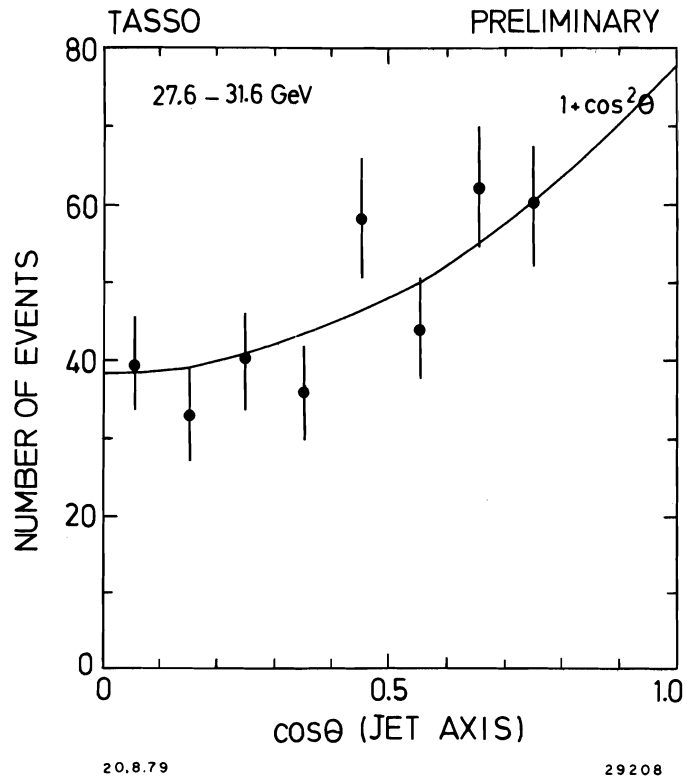


Fig.7 Angular distribution of the jet axis with respect to the beam.

not identified. Therefore the scaling variable $x = E/E_{\text{beam}}$ was replaced by $x_p = p/E_{\text{beam}}$ and the quantity $s d\sigma/dx_p$ was determined instead of $s/\beta d\sigma/dx$.

Corrections have been applied for acceptance, for radiative effects, for particle losses due to absorption and decay, and for electrons from the conversion of photons. These corrections were also applied for the single particle distributions shown later on.

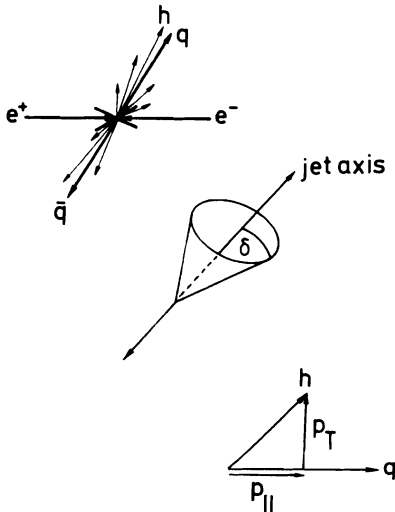
Fig.6 displays the TASSO data measured at 13, 17 and 27.4 - 31.6 GeV together with low energy measurements from DASP (5 GeV)⁸ and SLAC-LBL (7.4 GeV)¹¹. For $x > 0.2$ the TASSO cross sections are the same between 13 and 31.6 GeV and agree with those from 5 and 7.4 GeV to within $\sim \pm 30\%$, i.e. scaling is observed over this range of x and W with the accuracy specified. At low x the particle yield shows a dramatic rise from 5 to 30 GeV. This rise is related to the increase in multiplicity seen in Fig.5.

The 13 GeV data are somewhat special in that for $x > 0.2$ they are above the values measured for 17 GeV. Since 13 GeV is still close to the $b\bar{b}$ threshold this may indicate copious BB production (and decay).

Gluon emission will lead to scale breaking effects: the primary momentum is now shared by quark and gluon resulting in a depletion of particles at high x and an excess of particles at low x values. The curves in Fig.6 indicate the size of the expected scale breaking¹².

5. Jet Formation

The quark model views annihilation into hadrons as a two step process: first, a pair of quarks is produced which then fragment into hadrons.



If the hadron momenta transverse to the quark direction of flight are limited and the number of produced hadrons grows only logarithmically with energy the emitted hadrons will be more and more collimated around the primary quark directions as the total energy increases and one will observe jets. Let $\langle n \rangle = a + b \ln s$ be the average particle multiplicity, $\langle p_T \rangle$ and $\langle p_{||} \rangle \approx \langle p \rangle \approx \frac{\sqrt{s}}{\langle n \rangle}$ the average transverse and longitudinal momenta then the mean half angle of the jet cone is given by

$$\langle \delta \rangle = \frac{\langle p_T \rangle}{\langle p_{||} \rangle} \approx \frac{\langle p_T \rangle \cdot \langle n \rangle}{\sqrt{s}} \sim \frac{1}{\sqrt{s}} \quad (8)$$

In the present experiment jet formation was studied in terms of sphericity S ¹³ where the jet axis is determined by requiring $\sum p_{Ti}^2$ to be a minimum, and thrust T ¹⁴ where the jet axis is determined by maximizing $\sum |p_{||i}|$:

$$S = \frac{3}{2} \frac{\sum p_{Ti}^2}{\sum p_i^2} \quad 0 \leq S \leq 1 \quad (9)$$

$$T = \frac{\sum |p_{||i}|}{\sum p_i} \quad \frac{1}{2} \leq T \leq 1 \quad (10)$$

Extreme jettiness yields $S = 0$ and $T = 1$. Sphericity measures the square of the jet cone opening angle:

$$S \approx \frac{3}{2} \langle \delta^2 \rangle$$

likewise

$$T \approx \sqrt{1 - \langle \delta \rangle^2}$$

The data presented below were determined using only charged particles¹⁵. The results were generally found not to depend on whether the jet analysis was made with the sphericity or the thrust axis*). Monte Carlo studies with $q\bar{q}$ jets further showed that the jet axes so determined deviate by an average of less than 5° from the true axis above $W = 20$ GeV.

Test for quark jets

The polar angular distribution of the jet axis with respect to the beam is sensitive to the spin of the primary constituents:

$$\begin{aligned} W(\cos\theta) &\sim 1 + \cos^2\theta && \text{spin } 1/2 \\ &\sim 1 - \cos^2\theta && \text{spin } 0 \end{aligned}$$

Fig.7 shows $W(\cos\theta)$ summed over all data between 13 and 31.6 GeV. The data agree well with $W \sim 1 + \cos^2\theta$ and exclude a $1 - \cos^2\theta$ behaviour in agreement with the hypothesis that the primary constituents are a $q\bar{q}$ pair.

Fig.8 shows sphericity distributions for different energies between 13 and 31.6 GeV. The distributions shrink towards small S values as the energy increases. The curves show the prediction of the quark model with u, d, s, c and b quarks (dashed) plus gluon emission (solid). While at 13 and 17 GeV both models describe the data equally well at higher energies the QCD corrected curves agree somewhat better with the data.

In Fig. 9 the energy dependence of the average sphericity $\langle S \rangle$ is shown as measured in this experiment and by the PLUTO group¹⁶. The average sphericity decreases from 0.4 at the J/ψ to ~ 0.14 at 31.6 GeV. The trend to ever stronger collimation persists up to the highest energy explored in agreement with the simple quark model. The jet cone half opening angle drops from $\langle \delta \rangle \approx 31^\circ$ at 4 GeV to 17° at 31.6 GeV. The data of Fig.9 can be described by a straight line

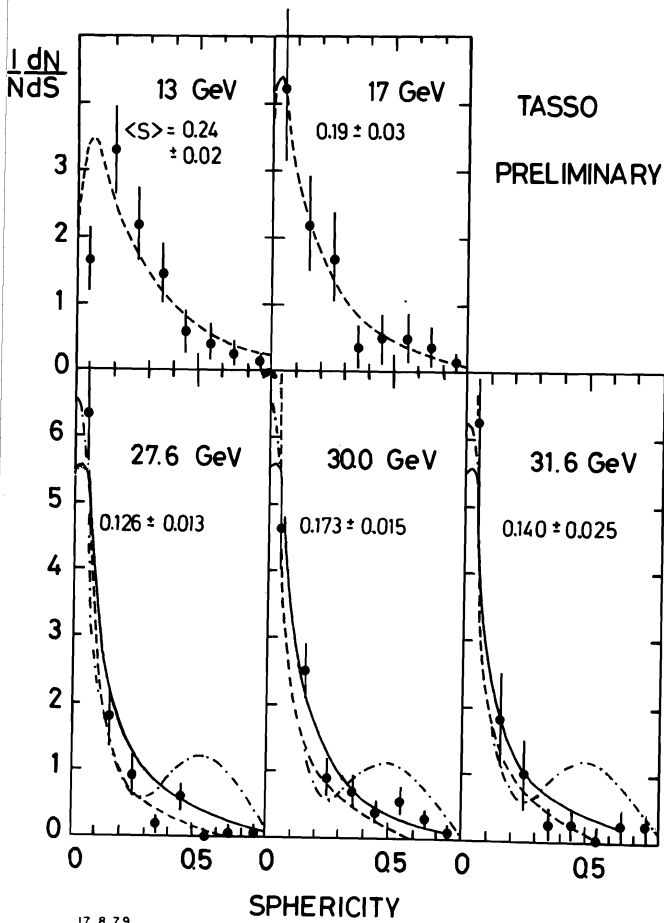
$$\langle S \rangle = 0.8 s^{-1/4}$$

The shrinkage of the jet cone is slower than expected from the simple reasoning given above which predicted $\langle S \rangle \sim s^{-1}$.

Similar conclusions can be drawn from the analysis of thrust. For completeness we give in Figs.10 and 11 the T distributions and the energy dependence of the average thrust $\langle T \rangle$.

Before analyzing the properties of jets in more detail we turn to the search for a new heavy quark. The event shape as measured e.g. by sphericity and thrust is particularly sensitive to a heavy quark contribution.

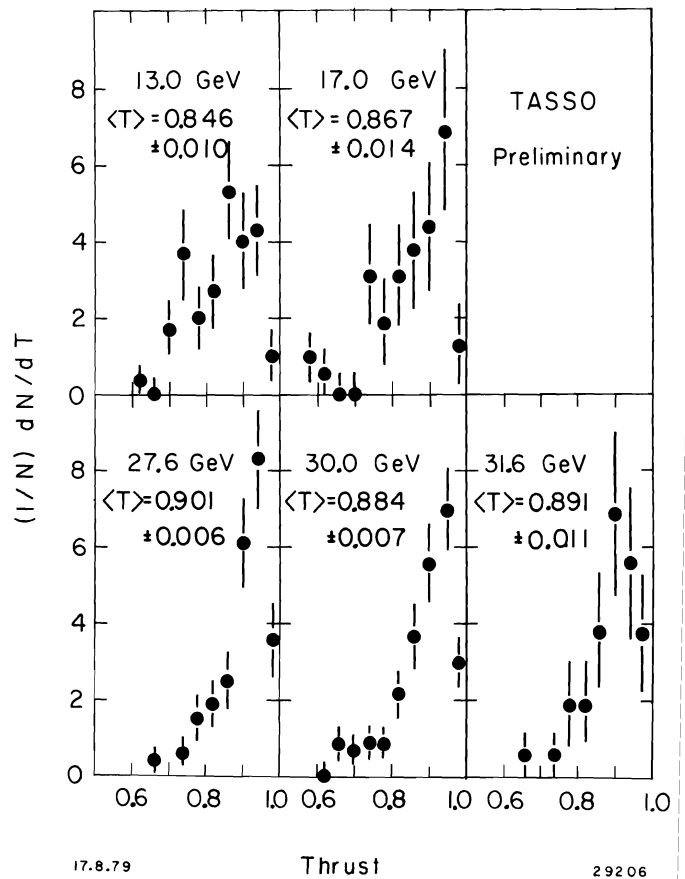
*) An exception is the "seagull effect" shown in Fig.17. Here only the thrust axis is useful since sphericity weighs fast particles too heavily and thus biases the particles of high $z = p/p_{\text{beam}}$ towards small values of p_T .



17.8.79

29207

Fig.8 Sphericity distributions for different c.m. energies. The curves show predictions of the quark model with u, d, s, c, b quarks (dashed) plus gluon corrections (solid) plus a t quark contribution (dashed-dotted).

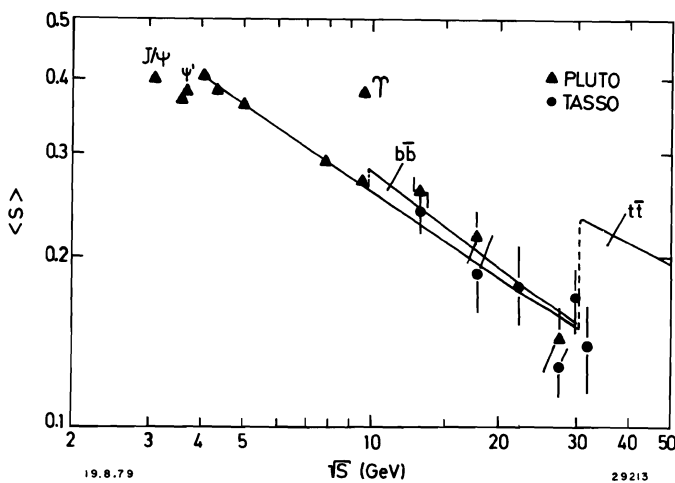


17.8.79

Thrust

29206

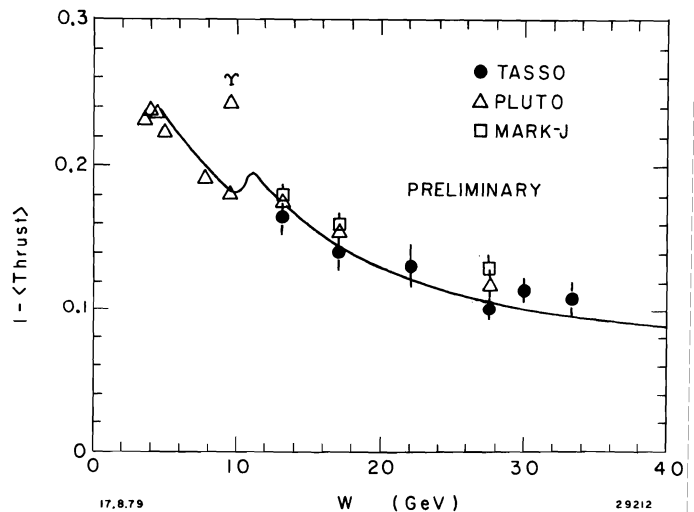
Fig.10 Thrust distribution for different c.m. energies.



19.8.79

29213

Fig.9 The average sphericity as a function of the c.m. energy. The curves indicate the expected contributions from u, d, s, c, b and t quarks including QCD corrections.



17.8.79

W (GeV)

29212

Fig.11 The average thrust as a function of the c.m. energy. The curve shows the theoretical prediction for u, d, s, c, b quarks plus QCD corrections (Ref. 23).

6. Search for New Heavy Quarks

The observed symmetry between leptons and quarks suggests besides u,d,s,c and b the existence of a sixth quark, t. The charge of the t quark is predicted to be +2/3 if one groups the quarks in weak isospin doublets, viz:

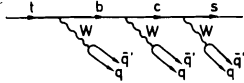
$$\begin{pmatrix} u \\ d \end{pmatrix}, \begin{pmatrix} c \\ s \end{pmatrix}, \begin{pmatrix} t \\ b \end{pmatrix}$$

The theoretical predictions for the t mass populate mass values between 10 and 40 GeV¹⁷. The observed spacing between ϕ , J/ψ and Υ would suggest for the mass of the $t\bar{t}$ vector ground state

$$m_{V_t} \approx m_{\Upsilon}^2 / m_{J/\psi} = 28 \text{ GeV}$$

which is in the reach of our experiment. Because of the (expected) narrow width of the V_t a fine energy scan is required to search for it. Such a scan has not yet been done. However the experiment is sensitive to the $t\bar{t}$ continuum. The continuum characterized by open t flavor production ($e^+e^- \rightarrow T\bar{T}$, where T is a $t\bar{q}$ meson, $q = u,d,\dots,b$) is expected to begin roughly 2 GeV above the vector ground state¹⁸. The asymptotic $t\bar{t}$ contribution to R should be $R_t = 3 \cdot (\frac{2}{3})^2 = \frac{4}{3}$. Near threshold it is likely to be larger. Comparing with the charm contribution near 4 - 4.5 GeV, one may expect $R_t \approx 2$. The R values shown in Fig.3 do not show this expected rise.

The event shape is more sensitive to the $t\bar{t}$ contribution. Events from $t\bar{t}$ decay can be expected to have a high multiplicity and a phase space like (spherical) configuration near threshold. According to the Kobayashi-Maskawa¹⁹ generalized Cabibbo matrix the favored decay sequence for t quarks is $t \rightarrow b + c + s$. As a consequence $T\bar{T}$ hadronic decays have no less than 14 (or more) quarks in the final state (see diagram)



Hadronic decay scheme for t quarks.

The production of $t\bar{t}$ events will lead to a step in the average sphericity $\langle S \rangle$ and to an accumulation of events at large S. The step in $\langle S \rangle$ can be readily calculated. The average S for phase space like events at 30 GeV is $\langle S_{PS} \rangle \approx 0.5$. The average S for the u,...,b contribution plus gluon corrections is $\langle S_{u,\dots,b} \rangle \approx 0.15$. Averaging over the two components predicts for $\langle S \rangle$ above the $t\bar{t}$ threshold

$$\langle S \rangle = \frac{R_t \langle S_{PS} \rangle + R_{u,\dots,b} \langle S_{u,\dots,b} \rangle}{R_t + R_{u,\dots,b}}$$

$$\geq 0.23$$

corresponding to a step of ≈ 0.08 . The data shown in Fig.9 do not show such a step. This is in line with the behaviour of the sphericity distributions which show no evidence for the accumulation of large S events expected from the $t\bar{t}$ contribution (dashed-dotted curves in Fig.8). The same conclusions are reached from the thrust distributions (Figs.10,11).

Sphericity measures the amount of collinearity (or the deviation from it). Two jet events are both collinear and planar while phase space like events at high energies are both noncollinear and nonplanar. For this

reason an inspection of the distribution of sphericity versus planarity will provide an even more stringent test on a $t\bar{t}$ (or any other heavy quark) contribution.

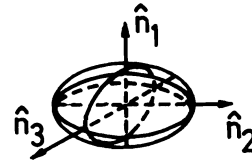
In order to study the shape of events we evaluate the momentum tensor ellipsoid (in analogy to the ellipsoid of the tensor of inertia). For each event one constructs the second rank tensor¹⁵ from the hadron momenta

$$M_{\alpha\beta} = \sum_{j=1}^N p_{j\alpha} p_{j\beta} \quad (\alpha, \beta = x, y, z) \quad (11)$$

summing over all N observed charged particles.

Let \hat{n}_1 , \hat{n}_2 and \hat{n}_3 be the unit eigenvectors of this tensor associated with the eigenvalues Λ_1 , Λ_2 and Λ_3 which are ordered such that $\Lambda_1 \leq \Lambda_2 \leq \Lambda_3$. Note that

$$\Lambda_i = \sum_j (p_j \hat{n}_i)^2$$



The principal axis is the \hat{n}_3 direction, the event plane is the \hat{n}_2, \hat{n}_3 plane and \hat{n}_1 defines the direction in which the sum of the square of the momentum components is minimized.

We define the normalized eigenvalues

$$Q_i = \frac{\Lambda_i}{\sum p_j^2} = \frac{\sum (\vec{p}_j \cdot \hat{n}_i)^2}{\sum p_j^2} \quad (12)$$

The Q_i satisfy the relation

$$Q_1 + Q_2 + Q_3 = 1$$

The events will be expressed in terms of the two variables aplanarity A and sphericity S

$$A = \frac{3}{2} Q_1 \quad (13)$$

$$S = \frac{3}{2} (Q_1 + Q_2) = \frac{3}{2} (1 - Q_3) \quad (14)$$

Since $0 \leq Q_1 \leq Q_2 \leq Q_3 \leq 1$ all events lie inside the triangle shown in Fig.12. The sketch shown in Fig.12a indicates the areas for collinear ($S \approx 0$) noncollinear coplanar ($S \neq 0, A \approx 0$) and for spherical events (S, A large). The event distribution shown in Fig.12b was obtained by summing over all data between 27.4 and 31.6 GeV. Few events are observed at large S and A. Fig.12c shows the event distribution expected in the case of a $Q\bar{Q}$ contribution where Q is a heavy quark. It was computed with a Monte Carlo program, assuming a quark mass of 10 GeV (this is a conservative assumption) and propagating the particles from Q fragmentation through the detector. Contrary to the expectation that all $Q\bar{Q}$ events should have (S,A) values close to that for spherical events (1, 0.5) the $Q\bar{Q}$ events populate rather uniformly the triangle plot. The reason for this is that the charged particle multiplicities are not infinite.

Assuming the $Q\bar{Q}$ contribution to have reached its asymptotic value $R_Q = 3 \cdot e_Q^2$, one can compare the observed and expected number of events for $e_Q = 2/3$ and $1/3$ for large values of A. This is done in Table 3. A t quark ($e = 2/3$) is clearly ruled out; also a

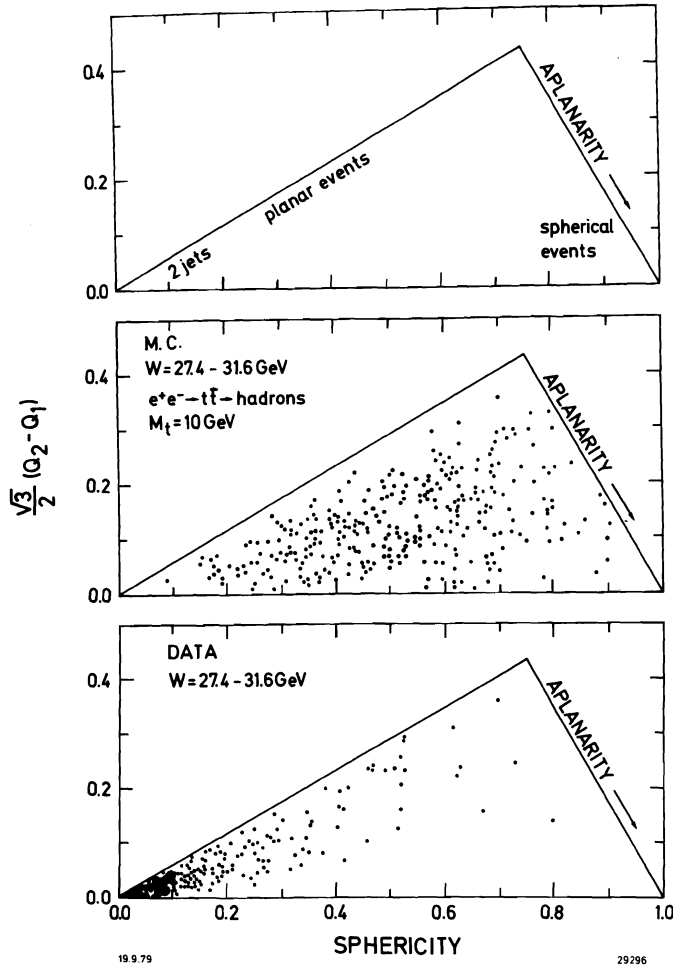


Fig.12 Distribution of events as a function of aplanarity

$$A = \frac{3}{2} Q_1 = \frac{3}{2} \frac{\langle p_T^2 \text{ out} \rangle}{\langle p^2 \rangle}$$

$$\text{and sphericity } S = \frac{3}{2} (Q_1 + Q_2) = \frac{3}{2} \frac{\langle p_T^2 \rangle}{\langle p^2 \rangle}$$

- (a) illustrating the regions for two jet, planar and spherical events
- (b) for Monte Carlo generated events from $t\bar{t}$ production, assuming a t mass of 10 GeV.
- (c) for real events at c.m. energies of 27.4 - 31.6 GeV.

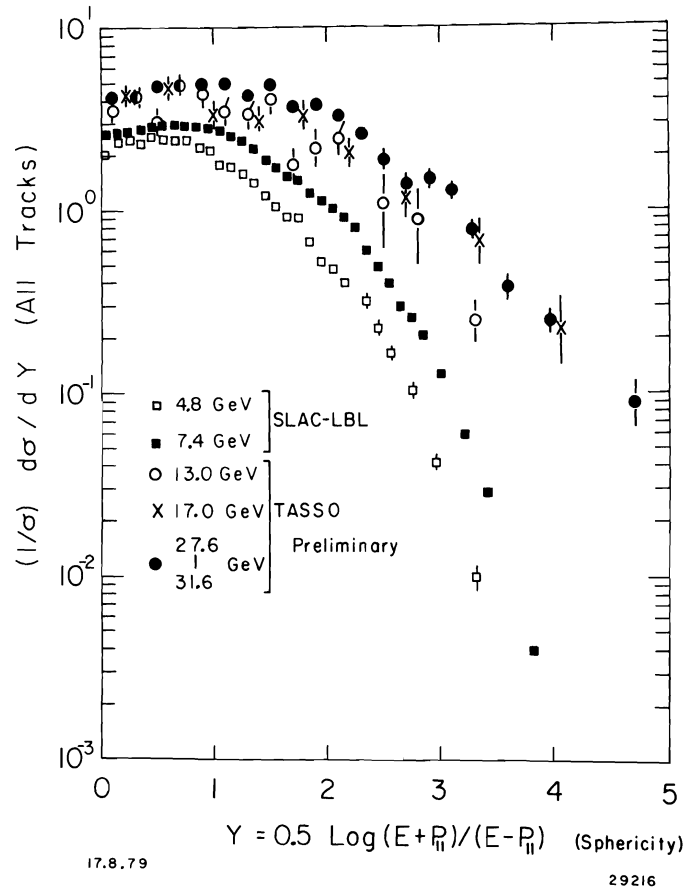


Fig.13 Rapidity distributions for charged particles assuming $m = m_t$, measured at 13, 17 and 27.4 - 31.6 GeV by this experiment and at 4.8 and 7.4 GeV by SLAC-LBL (Ref. 20).

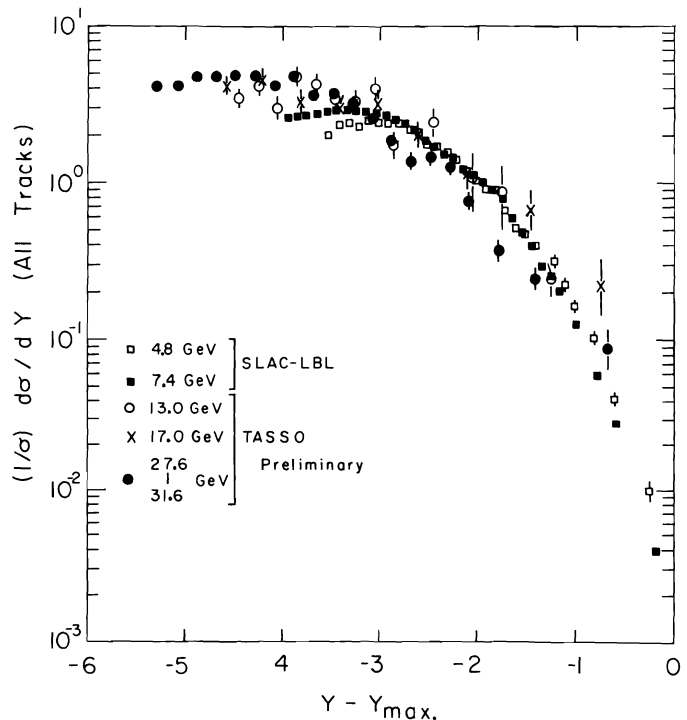


Fig.14 Rapidity distributions (same as in Fig.13) plotted as a function of $y - y_{\text{max}}$.

charge 1/3 quark contribution appears to be unlikely*. More precisely, the data exclude a possible $t\bar{t}$ continuum of strength $R_t = 4/3$ between $W = 20$ and 30 GeV.

Table 3: Search for a heavy quark Q contribution. Comparison of number of events for $A > 0.18$. The theoretical estimate assumes a Q mass of 10 GeV and $R_Q = 3 \cdot e_Q^2$.

e_Q	27.4 - 31.6 GeV	
	expected	observed
2/3	31	2
1/3	7.8	2

7. Longitudinal Momentum Distributions

The analysis of hadron production with respect to the jet axis permits in a clean manner a study of quark fragmentation since e.g. smearing effects due to quark fermi motion in the target are absent. The data were analysed in terms of the longitudinal and transverse momenta, $p_{||}$ and p_{\perp} , and the rapidity $y = 1/2 \ln \{(E + p_{||})/(E - p_{||})\}$.

Fig. 13 shows the rapidity distributions at 13, 17 and 27.4 - 31.6 GeV together with data from SLAC-LBL²⁰ measured at low energies (4.8 and 7.4 GeV). To compute y the particles were assumed to be pions. The normalization is to the total event yield (i.e. not per jet!). The width of the y distribution increases and some sort of plateau is developing as the energy increases. The height of the plateau is not constant but is rising too. The fragmentation region is approximately two units wide which is equal to what is observed in hadron scattering. The rapidity distribution in the fragmentation region within errors is the same between 4.8 and 17 GeV. However, the highest energy data (27.4-31.6 GeV) are lower, which may indicate scale breaking effects due to gluon bremsstrahlung. That can be seen when the data are plotted with respect to $y - y_{\max}$ ($y_{\max} \approx \frac{1}{2} \ln s/m^2$) as shown in Fig. 14.

Provided that only one kind of quark pair is produced and that the quarks fragment into pions only, theory predicts a plateau width Δy that grows logarithmically with energy,

$$\Delta y \approx y_{\max} - 2 \approx \frac{1}{2} \ln s/m^2 - 2$$

a constant plateau height and scaling in the fragmentation region. The experimentally observed rise of the height of the plateau is related to the more rapid growth of the average particle multiplicity above 10 GeV (see Fig.5) and is consistent gluon bremsstrahlung.

8. Transverse Momentum Distribution and Jet Broadening

The normalized transverse momentum distribution $d\sigma/dp_{\perp}^2$ evaluated with respect to the sphericity σ_{tot} axis is plotted in Fig.15 with respect to p_{\perp}^2 . The data at 13 and 17 GeV are identical within statistics and are averaged; similarly the data between 27.4 and 31.6 GeV are combined. The data for both energy regions are in reasonable agreement for $p_{\perp}^2 < 0.2$ (GeV/c)² but the high energy data are well above the low energy data for larger values of p_{\perp}^2 . The average value of p_{\perp}^2 increases from 0.15 ± 0.02 (GeV/c)² at 13, 17 GeV to 0.27 ± 0.02 (GeV/c)² at 27.4 - 31.6 GeV. The low energy data have been fitted for $p_{\perp}^2 < 1$ (GeV/c)² with the jet

* The conclusion on the production of a charge 1/3 quark Q rests on the assumption that the final states from $Q\bar{Q}$ on the average contain about the same number of charged particles as those from $t\bar{t}$. If $\langle n_{ch} \rangle$ is considerably less (say $\langle n_{ch} \rangle < 10$) the $Q\bar{Q}$ contribution becomes more difficult to observe.

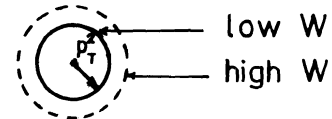
model of Field and Feynman extended to include c and b quarks. In this model the p_{\perp} distribution of the fragmented hadrons is governed by the parameter σ_Q ,

$$\frac{d\sigma}{dp_{\perp}^2} \sim e^{-\frac{p_{\perp}^2}{2\sigma_Q^2}}$$

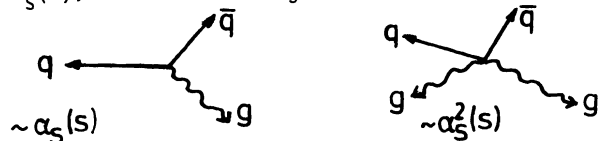
Increasing σ_Q from its original value⁴ of 0.25 GeV/c to 0.30 GeV/c leads to a good fit of the 13 + 17 GeV data (see Fig.15). To fit the higher energy data with the Field-Feynman model σ_Q must be increased to 0.45 GeV/c. This is in contradiction to the naive parton model which assumes the quark to fragment into hadrons with an energy independent transverse momentum distribution.

The widening of the transverse momentum distribution can have its origin in

1. the production of a new quark flavour. As discussed before the data do not show any evidence for the production of a new heavy quark and we can dismiss that as a possible explanation.
2. the p_{\perp} distribution for quark fragmentation into hadrons is energy dependent: the average p_{\perp} grows as the energy increases. In this case the hadrons are still produced in two jets but the diameter of the "cigar" in terms of p_{\perp} increases with energy (see sketch). Note also that both jets will grow in the same manner.



3. gluon bremsstrahlung from the outgoing quarks²¹⁻²⁷. The radiated gluon is expected to turn into a jet of hadrons. In QCD single gluon emission is proportional to $\alpha_s(s)$, double gluon emission proportional to $\alpha_s^2(s)$, etc. At low energies



where $\alpha_s(s)$ is of order one single as well as multi-gluon emission will be important. At our high energies where $s \approx 1000$ GeV and $\alpha_s(s) \ll 1$ (e.g. $\alpha_s(s = 1000 \text{ GeV}) = 0.2$ for $\Lambda = 0.5$ GeV) the emission of several hard gluons can be neglected. As a result there will be a tendency for only one jet to broaden. The $q\bar{q}g$ state is necessarily planar. This should reflect itself in the final hadron configuration which should retain the planarity with small transverse momenta with respect to the plane and large transverse momenta in the plane. The average transverse momentum of the gluon will rise linearly with energy,

$$\langle K_{\perp} \rangle \sim \alpha_s(s) \cdot W.$$

If K_{\perp} is large compared to the typical transverse momentum of 0.3 GeV/c, then the event will have a three jet topology²².

We shall now discuss the data. In Fig. 16 the average values of the longitudinal and transverse momentum are plotted as a function of c.m. energy. The average $p_{||}$ grows almost linearly with W . The transverse momentum shows a small but significant rise between 13 and 31.6 GeV. The average $\langle p_{\perp} \rangle$ is rapidly rising above 13 GeV. At 13 GeV the measured value is in accordance with the prediction of the $q\bar{q}$ model. At higher energies it is well above this prediction. However, gluon emission²⁷ describes the data rather well.

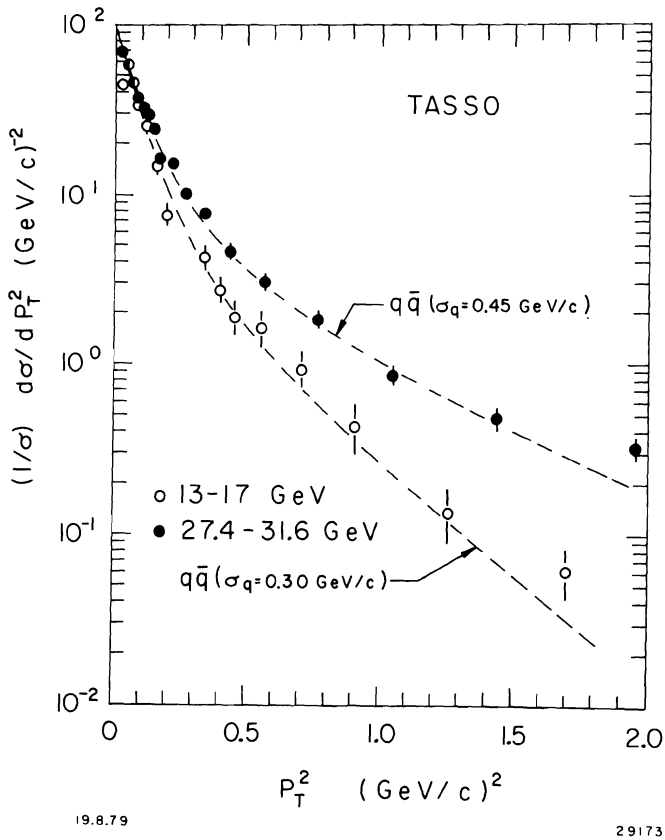


Fig.15 $1/\sigma_{tot} \frac{d\sigma}{dp_T^2}$ at 13 and 17 GeV (o) combined and for 27.4, 27.7, 30.0 and 31.6 GeV combined (●) as a function of p_T^2 . The curves are fits to the data for $p_T^2 < 1$ (GeV/c)² using the Field-Feynman quark-parton model including u,d,s,c and b quarks with σ_q as a free parameter.

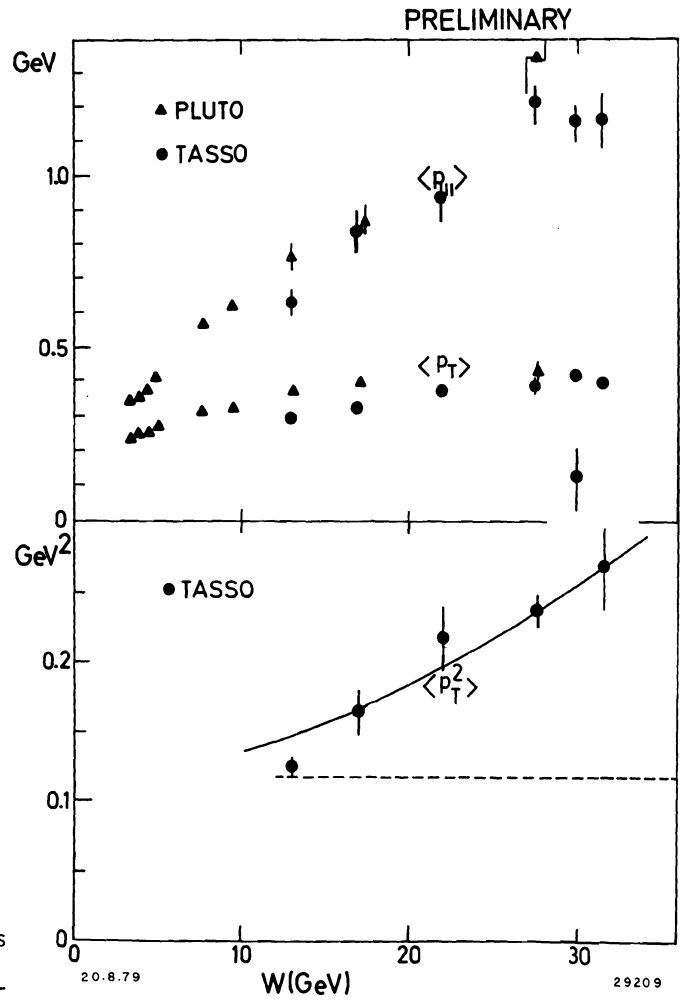


Fig.16 The energy dependence of $\langle p_{||} \rangle$, $\langle p_T \rangle$ and $\langle p_{\perp}^2 \rangle$ relative to the thrust axis for charged particles. The curves show the prediction for $q\bar{q}$ (dashed) and $q\bar{q}$ + gluon production (Ref.27).

In Fig.17 each event was divided into two halves by a plane perpendicular to the jet axis and $\langle p_T^2 \rangle$ was determined separately for the two sides. The jet with the smaller $\langle p_T^2 \rangle$ was called the narrow jet, the other one the wide jet. Then p_T^2 was determined as a function of $z = p/p_{\text{beam}}$ and averaged over all narrow and wide jets, respectively. The result (also called the seagull plot) is shown in Fig.17 separately for 13, 17 GeV and 27.4 - 31.6 GeV. The wide jet has larger $\langle p_T^2 \rangle$ values than the narrow one. The qq model with $\sigma_q = 0.3$ GeV/c fits the low energy data rather well which implies that there the narrow-wide asymmetry is due to statistical fluctuations. The model fails to describe the high energy data which would mean that there a genuine narrow/wide asymmetry exists. However, increasing σ_q to 450 MeV/c, obtained from the fit to the p_T^2 distribution, approximately reproduces the data. Therefore we can fit both the p_T^2 distributions and the seagull plot at both energies by increasing the value of σ_q with energy.

Next we study the event shapes using the method introduced already in sect.6. In Fig.18 we compare the distribution of

$$\langle p_T^2 \rangle_{\text{out}} = \frac{1}{N} \sum_{j=1}^N (\vec{p}_j \cdot \hat{n}_1)^2$$

(= square of the momentum component normal to the event plane given by \hat{n}_2 and \hat{n}_3)

with that of

$$\langle p_T^2 \rangle_{\text{in}} = \frac{1}{N} \sum_{j=1}^N (\vec{p}_j \cdot \hat{n}_2)^2$$

(= square of the momentum component in the event plane perpendicular to the jet axis). The data show little increase in $\langle p_T^2 \rangle_{\text{out}}$ from low to high energy. The distribution of $\langle p_T^2 \rangle_{\text{in}}$, however, becomes much wider at high energies, and in particular there is a long tail of events with a large value of $\langle p_T^2 \rangle_{\text{in}}$ not observed at low energies. The curves show the expectations from the Monte Carlo qq jet. Hadrons resulting from pure qq jets will on the average be distributed uniformly around the jet axis. However, some asymmetry between $\langle p_T^2 \rangle_{\text{out}}$ and $\langle p_T^2 \rangle_{\text{in}}$ is caused by statistical fluctuations. Fair agreement with the qq model is found for both $\langle p_T^2 \rangle_{\text{out}}$ and $\langle p_T^2 \rangle_{\text{in}}$ at the low energy point. Thus the asymmetry observed at this energy can be explained by statistical fluctuations alone.

At the high energy, we find fair agreement between $\langle p_T^2 \rangle_{\text{out}}$ and the qq model with $\sigma_q = 0.3$ GeV/c, however, the long tail of the $\langle p_T^2 \rangle_{\text{in}}$ distribution is not reproduced by the model. This discrepancy cannot be removed by increasing σ_q . The result with $\sigma_q = 0.45$ GeV/c is also plotted in Fig.18. The agreement is poor. We therefore conclude that the data include a number of planar events that are not reproduced by the qq model independent of the assumption on the average p_T in that model.

Fig.19 shows the distribution of aplanarity A versus sphericity S for low and high energies. Collinear two-jet events are seen to dominate at all energies. We exclude the collinear events by requiring $S > 0.25$ and subdivide the events into planar and nonplanar events requiring $A \geq 0.04$. Table 4 lists the number of events observed together with the predictions of the qq model for $\sigma_q = 0.30$ GeV/c and 0.45 GeV/c and for qq production with gluon bremsstrahlung (qqg). The gluon fragmentation function - which is unknown - was assumed to be the same as for quarks (with $\sigma_q = 0.3$ GeV/c). Because of the uncertainty in the gluon fragmentation function the qqg numbers given in Table 4 can only be regarded as indicative.

Table 4: Comparison of the observed number of non-collinear events with the qq and qqg predictions for 27.4 - 31.6 GeV.

	observed	$\sigma_q = 0.30$ GeV/c	$\sigma_q = 0.45$ GeV/c	qqg ²⁷
noncollinear planar events S>0.25, A<0.04	18	4.5	4.5	~17
noncollinear nonplanar events S>0.25, A>0.04	38	32	38	~35

At low and high energies the number of observed non-collinear-nonplanar events can be understood in terms of the qq or qqg models. That is to say, no new mechanism has to be invoked that produces a large number of noncollinear events together with a spill-over into the planar region. The number of planar events observed at 13, 17 GeV is not too far from the qq prediction. At the high energies we find 18 events compared with 4.5 events predicted by the qq model independent of σ_q . An independent test of the planar structure was made in the following way: All tracks were rotated around the sphericity axis by a random azimuthal angle. This preserves $p_{||}$ and p_T . Then the sign of $p_{||}$ was changed at random, too. This procedure destroys any natural correlations. As a result 6 randomized events were found in the planar region at 13, 17 GeV and 4 events at 27.4 - 31.6 GeV. Thus at the high energies there is an excess of planar events well above the level predicted from statistical fluctuations of qq jets. This shows that $e^+e^- \rightarrow$ hadrons proceed via the creation and decay of at least three primary constituents that subsequently fragment into hadrons. The number of planar events observed is consistent with the gluon bremsstrahlung process.

If gluon bremsstrahlung is the correct explanation and if the gluon materializes as a jet of hadrons with limited transverse momentum then a small fraction of the events should display a three-jet structure. The events were analysed for a three jet structure using the procedure described in ref. 28. All planar events gave a good fit to the three jet hypothesis. To compare the class of three-jet events with the predominant class of two-jet events Fig.20 shows characteristic events of each type in momentum space in all three projections. Figs.20a,d,g show the momenta projected into the $\hat{n}_2 - \hat{n}_3$ plane (event plane); this is the plane containing the largest components of momenta. The first event shows two clearly delineated jets. The three-jet events, on the other hand, show a much broader distribution of momenta transverse to the \hat{n}_3 axis. Fig.20b,e show the projection onto the plane perpendicular to the jet axis (\hat{n}_2). Here one clearly sees the small transverse momenta of the two-jet event and the tendency of the large transverse momentum to lie along the \hat{n}_2 direction for the three-jet events. Finally Figs.20c,f show the projection onto the $\hat{n}_1 - \hat{n}_3$ plane.

9. Characteristics of the Planar Events.

We have studied the characteristics of the planar events defined by $S > 0.25$, $A < 0.04$ at 27.4 - 31.6 GeV.

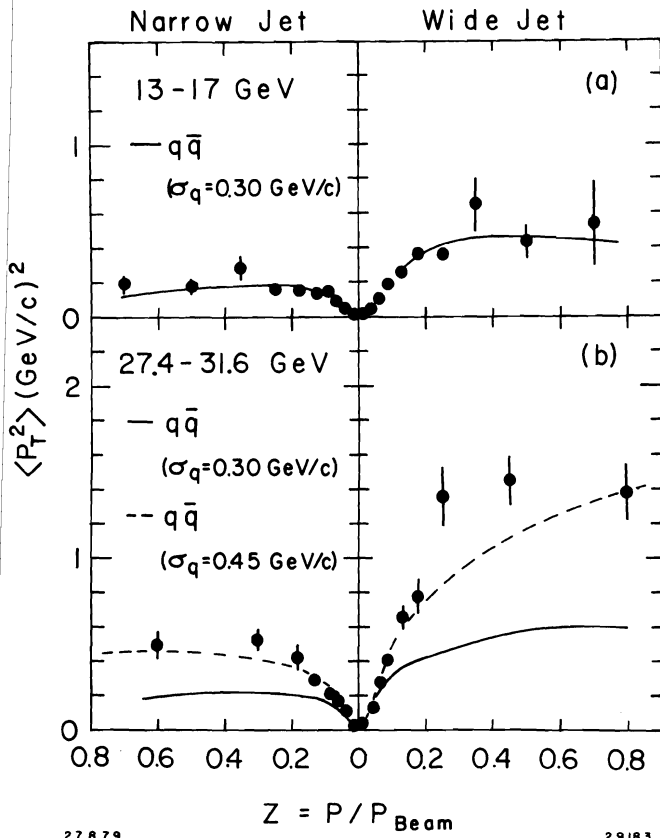


Fig.17 Average p_T^2 for charged hadrons with respect to the jet axis as a function of the fractional hadron momentum $z = P/P_{\text{beam}}$ separately for the narrow and the wide jet.

(a) for 13, 17 GeV combined

(b) for 27.4 - 31.6 GeV combined.

The curves show the prediction of the $q\bar{q}$ model with $\sigma_q = 0.3 \text{ GeV/c}$ (solid) and 0.45 GeV/c (dashed). The model includes u,d,s,c,b quarks.

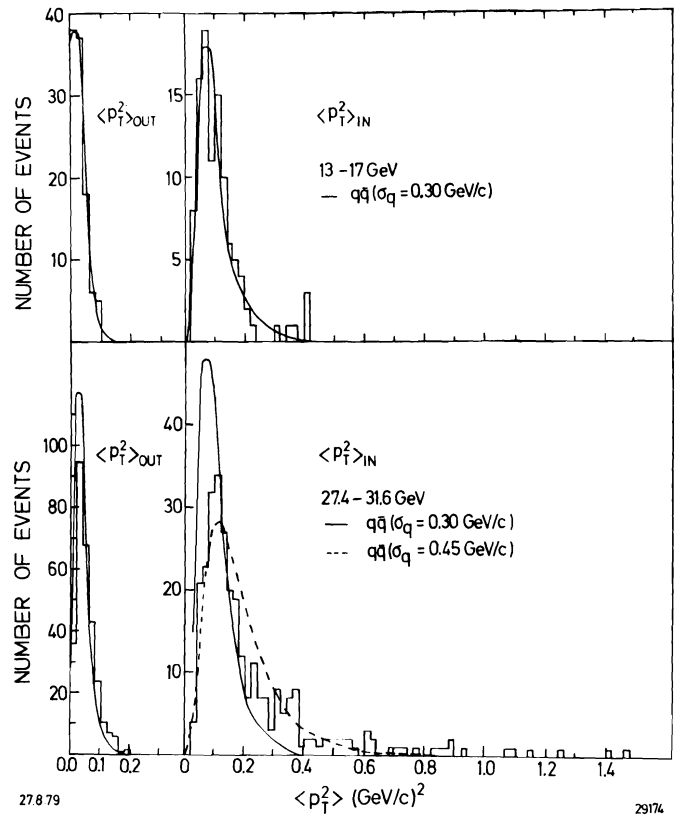


Fig.18 The mean transverse momentum squared normal to the event plane $\langle p_T^2 \rangle_{\text{OUT}}$ and in the event plane $\langle p_T^2 \rangle_{\text{IN}}$ per event for the low and the high energy data. The curves show the predictions of the $q\bar{q}$ model with $\sigma_q = 0.3 \text{ GeV/c}$ (solid) and 0.45 GeV/c (dashed).

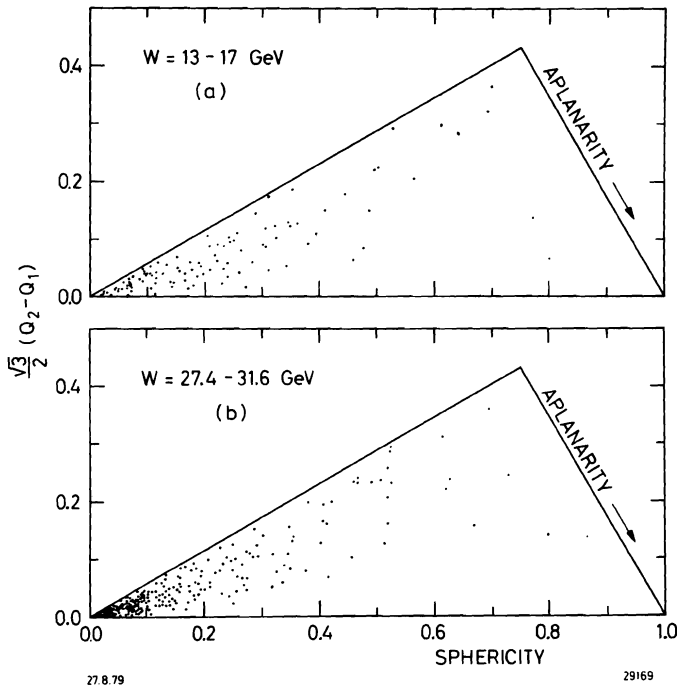
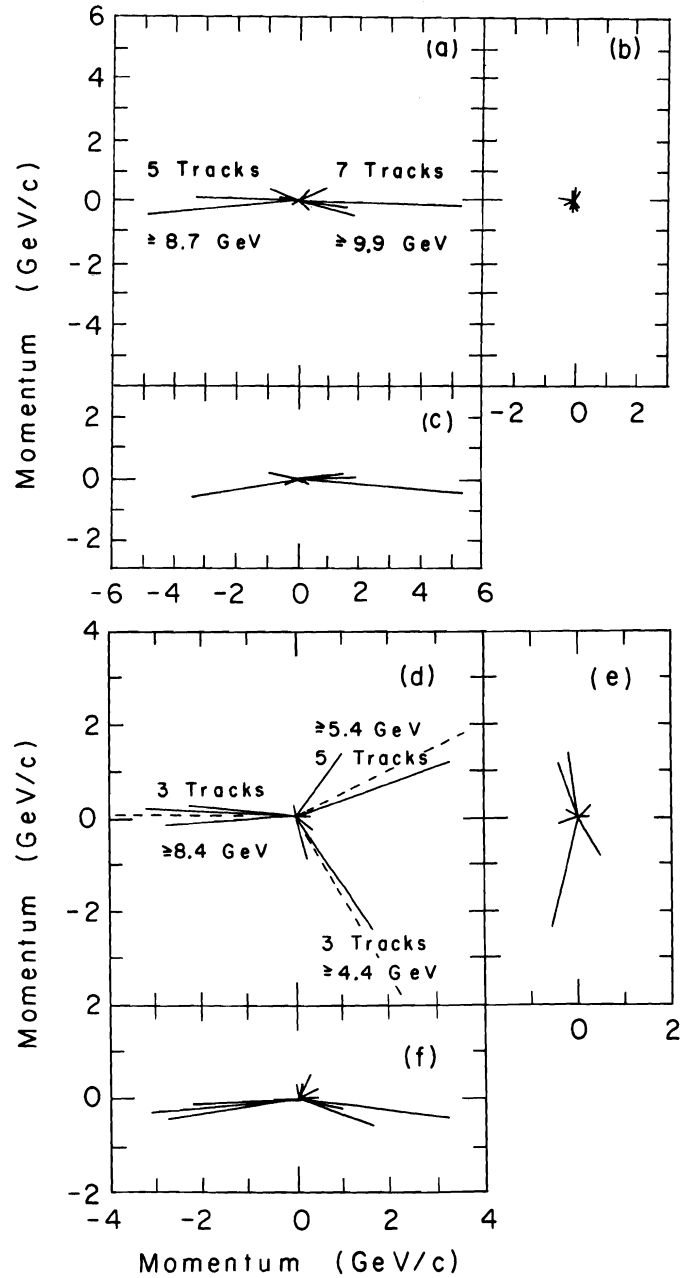


Fig.19 Distribution of the events as a function of aplanarity

$$A = \frac{3}{2} Q_1 = \frac{3}{2} \frac{\langle p_T^2 \text{ out} \rangle}{\langle p^2 \rangle} \quad \text{and sphericity}$$

$$S = \frac{3}{2} (Q_1 + Q_2) = \frac{3}{2} \frac{\langle p_T^2 \rangle}{\langle p^2 \rangle} \quad \text{for the low (a) and high (b) energy data.}$$



23.8.79

29184

Fig.20 Momentum space representation of a 2-jet event (a-c) and a 3-jet event (d-f) in each of three projections.

(a,d) = $\hat{n}_2 - \hat{n}_3$ plane

(b,e) = $\hat{n}_1 - \hat{n}_2$ plane

(c,f) = $\hat{n}_1 - \hat{n}_3$ plane.

The dotted lines show the fitted jet axes.

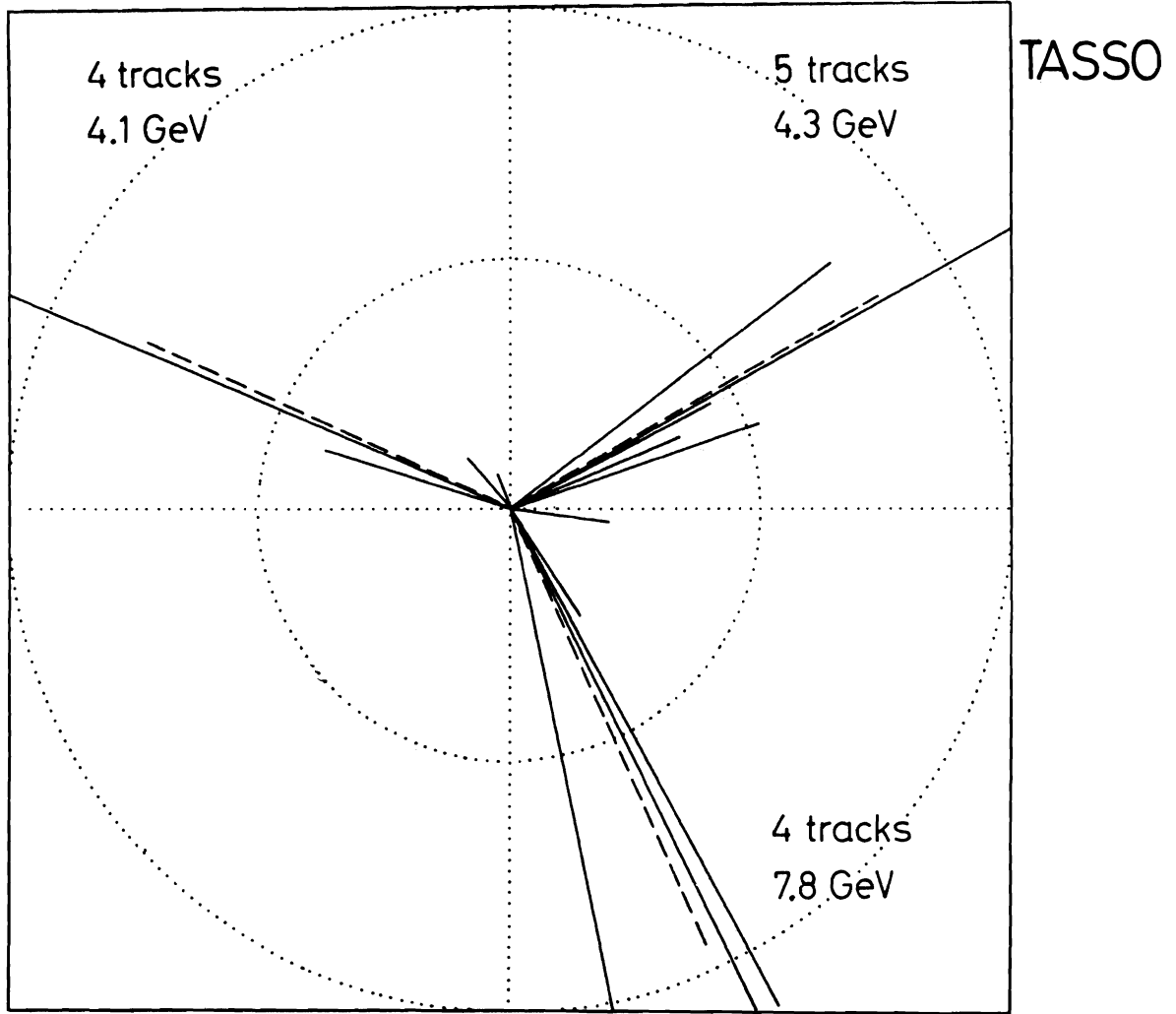


Fig.20g Another 3-jet event projected into the event plane.

In Fig.21 the distribution of the sum of the observed charged particle momenta, Σp_i , for planar events (cross hatched histogram) is compared to the distribution for all events (open histogram). Within statistics the planar events have the same Σp_i distribution as the total event sample. If the planar events would e.g. originate from two-photon processes or from radiative processes where the incident electron or positron has emitted a high energy photon, they would cluster near low Σp_i values.

Fig.22 compares the charged particle multiplicity distribution for planar and for all events. No significant difference is observed.

The planar events were analysed as three jet events and the average p_T per jet was measured. Fig.23 shows the observed $\langle p_T \rangle$ distribution. The average p_T value is 0.3 GeV/c. Hence the planar events which lead to large $\langle p_T \rangle$ values when treated as two-jet events have the canonical $\langle p_T \rangle$ value of ~ 0.3 GeV/c when analysed as three-jet events.

10. Conclusions

1. The ratio R of the total cross section for e^+e^- annihilation into hadrons to the μ pair cross section is constant within errors between c.m.energies of 17 and 31.6 GeV and has a value close to 4.
2. No evidence has been found for the t quark. It appears unlikely that the threshold for continuum $t\bar{t}$ production is below 30 GeV.
3. The multiplicity for charged particles above 10 GeV is found to rise faster than at lower energies.
4. The cross section quantity $s \frac{d\sigma}{dx}$ scales for $x > 0.2$ and $W \geq 5$ GeV to within ± 30 %.
5. The shape and magnitude of the total cross section, the observed scaling of $s \frac{d\sigma}{dx}$, the occurrence of jets and their gross features are in astonishing agreement with the quark hypothesis.

However:

6. The transverse momentum distribution of hadrons relative to the jet axis broadens with increasing energy: $\langle p_T^2 \rangle$ rises rapidly. Hence in the qq model the fragmentation function is not energy dependent.
7. The increase of $\langle p_T^2 \rangle$ occurs primarily in only one of the two jets. The distribution of the transverse momentum perpendicular to the "event plane" does not show a pronounced energy dependence while a strong broadening takes place in the event plane at the highest values of $s (= Q^2) \approx 1000 \text{ GeV}^2$.
8. We observe planar events at a rate which is well above the rate computed for statistical fluctuations of the qq jets.
9. The planar events when analysed as three-jet events yield an average transverse momentum of 0.3 GeV/c relative to the jet axis.
10. The planar events establish in a model independent way that a small fraction of the e^+e^- annihilation events proceeds via the emission of three constituents, each of which materializes as a jet of hadrons in the final state.

The data are most naturally explained by hard non-collinear gluon bremsstrahlung, $e^+e^- \rightarrow qqg$.

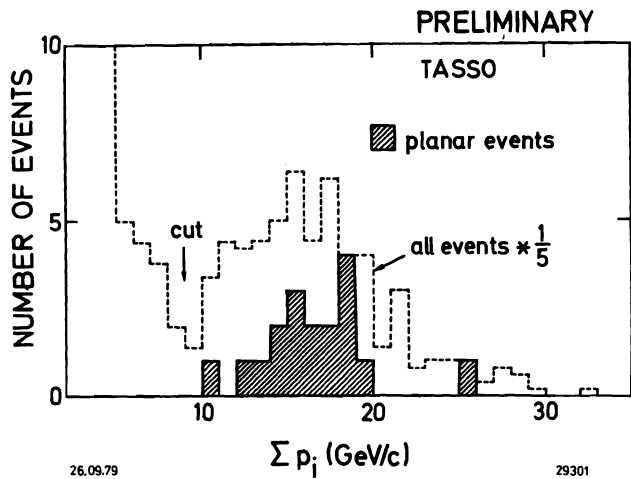


Fig.21 Distribution of the total visible momentum of hadron events.
 Cross hatched histogram: for noncollinear planar events ($S > 0.25$, $3/2 Q_1 < 0.04$)
 open histogram: all events; the number of events has been reduced by a factor 5.

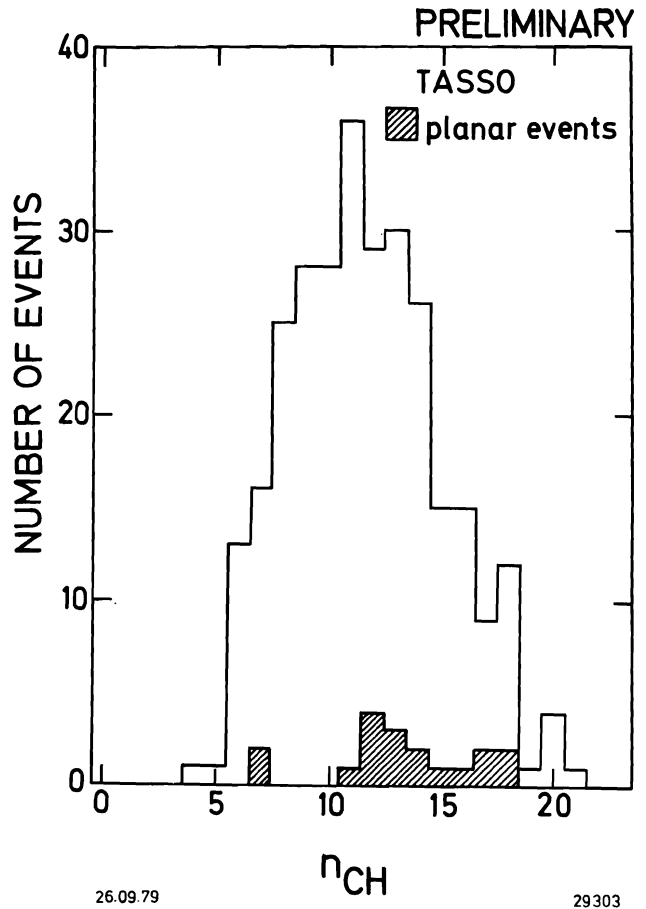


Fig.22 Distribution of the observed charged particle multiplicity for noncollinear planar events ($S > 0.25$, $3/2 Q_1 < 0.04$), cross hatched histogram, and for all events, open histogram.

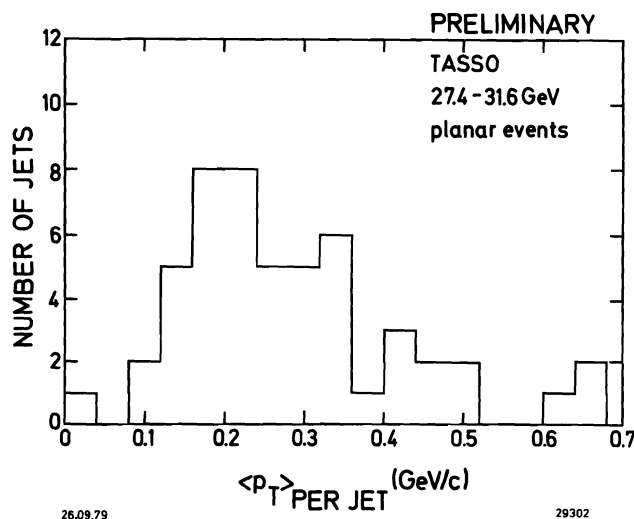


Fig.23 Distribution of the average p_T per jet for noncollinear planar events ($S > 0.25$, $3/2 Q_1 < 0.04$) analysed as three jet events.

List of References

1. The members of the TASSO Collaboration are:
 R.Brandelik, W.Braunschweig, K.Gather, V.Kadansky,
 K.Lübelmeyer, P.Mättig, H.-U. Martyn, G.Peise,
 J.Rimkus, H.G.Sander, D.Schmitz, A.Schultz von
 Dratzig, D.Trines, W.Wallraff
 I. Physikalisches Institut der RWTH Aachen, Germany
 H.Boerner, H.M.Fischer, H.Hartmann, E.Hilger, G.Knop,
 W.Korbach, P.Leu, B.Löhr, F.Roth, W.Rühmer, R.Wede-
 meyer, N.Wermes, M.Wollstadt
 Physikalisches Institut der Universität Bonn,
 Germany
 R.Bühring, R.Fohrmann, D.Heyland, H.Hultschig,
 P.Joos, W.Koch, U.Kötz, H.Kowalski, A.Ladage,
 D.Lüke, H.L. Lynch, G.Mikenberg, D.Notz, J.Pyrlik,
 R.Riethmüller, M.Schliwa, P.Söding, B.H.Wiik,
 G.Wolf
 Deutsches Elektronen-Synchrotron DESY, Hamburg,
 Germany
 M.Holder, G.Poelz, J.Ringel, O.Römer, R.Rüsch,
 P.Schmüser
 II. Institut für Experimentalphysik der Universität
 Hamburg, Germany
 D.M.Binnie, P.J.Dornan, N.A.Downie, D.A.Garbutt,
 W.G.Jones, S.L.Lloyd, D.Pandoulas, A.Pevsner,
 J.Sedgebeer, S.Yarker, C.Youngman
 Department of Physics, Imperial College London,
 England
 R.J.Barlow, R.J.Cashmore, J.Illingworth, M.Ogg,
 G.L.Salmon
 Department of Nuclear Physics, Oxford University,
 England
 K.W.Bell, W.Chinowsky, B.Foster, J.C.Hart, J.Proud-
 foot, D.R.Quarrie, D.H.Saxon, P.L.Woodworth
 Rutherford Laboratory, Chilton, England
 Y.Eisenberg, U.Karshon, E.Kogan, D.Revel, E.Ronat,
 A.Shapira
 Weizmann Institute, Rehovot, Israel
 J.Freeman, P. Lecomte, T.Meyer, Sau Lan Wu,
 G.Zobernig
 Department of Physics, University of Wisconsin,
 Madison, Wisconsin, USA
2. B.H.Wiik, Proceedings of the International Neutrino
 Conference, Bergen, Norway, 18-22 June 1979.
 R.Cashmore, Proceedings of the EPS International
 Conference on High Energy Physics, Geneva, Switzer-
 land, 27 June - 4 July 1979 and DESY-Report 79/50
 P.Söding, *ibid.*
 G.Wolf, *ibid.* and DESY-Report 79/14 (1979)
3. TASSO Collaboration, R.Brandelik et al., Phys.Lett.
83B (1979) 261
4. B.Anderson et al., Nucl.Phys. B135 (1978) 273;
 R.D.Field and R.P.Feynman, Nucl.Phys. B136 (1978) 1
 The Monte Carlo program was modified by T.Meyer to
 include besides u,d,s the pairproduction of c and b
 quarks.
5. G.Bacci et al., Frascati report LNF 79/34 (1979);
 G.P.Murtas, 1978 Tokyo Conference, B2
6. SLAC-LBL Collaboration, G.G.Hanson, 13th Rencontre
 de Moriond (1978) ed. by J.Tran Thanh Van, Vol.II
7. PLUTO Collaboration, Ch.Berger et al., Phys.Lett.
81B (1979) 410 and
 V. Blobel, private communication
8. DASP Collaboration, R.Brandelik et al., Nucl.Phys.
B148 (1979) 189
9. E.Albini, P.Capiluppi, E.Giacomelli and A.M.Rossi,
 Nuovo Cimento 32A (1976) 101
10. S.D.Drell, D.Levy and T.M.Yan, Phys.Rev. 187 (1969)
 2159
11. R.F.Schwitters, rapporteur talk, 1975 Stanford
 Conference, p.5
12. R.Baier, J.Engels and B.Peterson, University of
 Bielefeld report BI-TP 79/10 (1979) and
 B.Peterson, private communication;
 W.R.Frazer and J.F.Gunion, University of California
 report UCD-78-5 (1978), and J-F.Gunion, private
 communication
13. J.D.Bjorken and S.J.Brodsky, Phys.Rev. D1 (1970)
 1416;
 G.Hanson et al., Phys.Rev.Lett. 35 (1975) 1609
14. S.Brandt et al., Phys.Lett. 12 (1964) 57;
 A. De Rujula, J. Ellis, E.G.Floratos, and M.K.Gail-
 lard, Nucl.Phys. B138 (1978) 387;
 E.Fahri, Phys.Rev.Lett. 39 (1977) 1587
15. TASSO Collaboration, R.Brandelik et al., DESY Report
 79/53 (1979) and Phys.Lett., to be published.
16. PLUTO Collaboration, V.Blobel, data reported at the
 EPS International Conference on High Energy Physics,
 Geneva, Switzerland, 27 June - 4 July 1979
17. see e.g. C.J.Aubrecht II and D.M.Scott, C00-1545-
 247;
 G.Preparata, CERN TH 2599 (1978);
 M.A.Combrugghe, Phys.Lett. 80B (1979) 365;
 H.Georgi and D.V.Nanopoulos, HUTH-78/A039 (1978);
 H.Harari, H.Haut and J.Weyers, Phys.Lett. 78B (1978)
 459;
 J.D.Bjorken, SLAC-PUB-2195 (1978);
 T.F.Walsh, DESY-Report DESY 78/68 (1978);
 T.Kitazoe and K.Tanaka, Phys.Rev. D18 (1978) 3476;
 S.Pakvasa and H.Sugawara, Phys.Lett. 82B (1979) 105
18. C.Quigg and J.C.Rosner, Phys.Lett. 72B (1978) 462;
 G.Bhanot and S.Rudaz, Phys.Lett. 78B (1978) 119;
 H.Krasemann and S.Ono, DESY-Report DESY 79/9 (1979)
19. M.Kobayashi and K.Maskawa, Prog.Theor.Phys. 49
 (1973) 652
20. G.G.Hanson, 13th Rencontre de Moriond (1978), ed.by
 J.Tran Thanh Van, Vol. II
21. J.Kogut and L.Susskind, Phys.Rev. D9 (1974) 697,
 3391;
 A.M.Polyakov, Proc. 1975 Int.Symp. on Lepton and
 Photon Interactions at High Energies, Stanford, ed.
 by W.T.Kirk, p. 855
22. J.Ellis, M.K.Gaillard and G.G.Ross, Nucl.Phys. B111
 (1976) 253, erratum B130 (1977) 516
23. A. de Rujula, J.Ellis, E.G.Floratos and M.K.Gail-
 lard, Nucl.Phys. B138 (1978) 387
24. T.A. de Grand, Y.J.Ng and S.-H.H.Tye, Phys.Rev. D16
 (1977) 3251
25. G.Sterman and S.Weinberg, Phys.Rev.Lett. 39 (1977)
 1436
26. G.Kramer and G.Schierholz, DESY-Report DESY 78/62
 (1978)
 G.Kramer, G.Schierholz and J.Willrodt, Phys.Lett.
 79B (1978) 249
27. P.Hoyer, P.Osland, H.G.Sander, T.F.Walsh and
 P.M.Zerwas, DESY-Report DESY 79/21 (1979)
28. S.L.Wu and G.Zobernig, Particles and Fields
 (Z.Physik C) 2 (1979) 107.

G. Wolf

Speaker: Tannenbaum - Rockefeller University

- Q. As you say, p_t broadening is correlated with high z . Did you ever do it versus rapidity, since you show rapidity plots? Did you look at that?
- A. Yes.
- Q. What did it look like?
- A. It is also broadened. The broadening occurs basically in the fragmentation region.

Speaker: A. Odian - SLAC

- Q. Do you have multiplicity distributions?
- A. Yes, see Fig. 22 showing the high energy data.
- Q. As a function of energy?
- A. Of energy? No, I don't have it with me.

Speaker: Fred Messing - Carnegie Mellon

- Q. Another way to look for the top quark would be to look for an increase in strange particle production indicated by your decay scheme.
- A. Yes.
- Q. Would you like to make a comment on this?
- A. No.

Speaker: ?

- Q. In reference to the cross section $sd\sigma/dx$, with which Λ value was the QCD prediction calculated?
- A. The curve I showed was computed with $\Lambda = 500$ MeV.
- A. I showed the amount of scale breaking one expects with QCD if $\Lambda = 500$ MeV is assumed. We have not done the inverse: to find out what range of Λ values is allowed by the data.

Speaker: ?

- Q. Could you give us a short status report of the aerogel counter?
- A. For one hadron arm, 1/2 of the Cerenkov counters has already been installed about 4 months ago. The second arm is being installed right now. At the end of September we will have about 3/4 of the Cerenkov system (aerogel + gas counters) installed.

Speaker: Ronan - LBL

- Q. Could you review the evidence to why the p_t broadening is a high- z effect?
- A. Fig. 17 shows that the tracks with large p_t^2 have also large z ($z > 0.2$).

Speaker: Minh - LASL

- Q. Since you want to study systematically the effects of the QCD scale breaking phenomenon, is it not better to plot the scaling cross section as a function of the longitudinal momentum, that is the projection along the jet axis rather than the total momentum?
- A. The structure functions $\overline{W}_1, \overline{W}_2$ are functions of x and not of $x_{||}$.

Speaker: Karl - Guelph

- Q. Did you look at the charged energy distribution as a function of center of mass energy? What is the fraction of total energy carried by charged particles?
- A. Fig. 3 shows for a c.m. energy of 30 GeV the sum of the momenta of charged particles. The average value is near 15 GeV. In other words, 50 % of the total energy is in the charged particles.
- Q. Did you look at the variation with the center of mass energy?
- A. The fraction is approximately the same for the lower energies.